

LOAD TRANSFER OF PASSANGER CAR COMPARTMENT FOR IMPROVEMENT OF STRUCTURAL PERFORMANCE IN SIDE IMPACT

Satoshi Akima

Keio University, Graduate School of Science and Technology
Japan

Masaki Omiya

Kunihiro Takahashi

Keio University
Japan

Paper Number 15-0209

ABSTRACT

We demonstrate the effectiveness of a new method for expressing the load transfer in passenger car bodies to improve structural performance in order to protect occupants in side impact. For vehicle structures, one of the most important goals is the reduction of compartment deformation. For this purpose, indicating the load transfer paths in a vehicle compartment is fundamentally significant. The present authors previously developed an index Ustar (U^*) to express the load paths in structures. Our purpose in the present study is to express the load transfer using U^* in a vehicle compartment in side impact.

The index U^* is defined as $U^* = 1 - U/U'$, where U is the work done at the loading point and U' is the work done when an arbitrary point is constrained. We can say that U^* shows the connectivity between the loading point and an arbitrary point. It is natural to think that the force is transferred along the highest part of the U^* distribution. The index U^* can realize a way to obtain the overall view of load transfer in the vehicle compartment during collisions.

We introduce the extended U^* in which the effect of inertial force is included for the calculation of vehicle collision. The calculated distribution of U^* for a sample passenger car shows that the impact force is transferred mainly to the lower structure of the compartment. However, the load is not transferred to the opposite body side, because of the separation caused by the center tunnel structure. The U^* distribution shows that among the several transverse cross-members, the cross-member under the B-pillar plays a key role in load transfer. In contrast, the cross-member under the front seat has a small effect for load transfer. These results of load transfer are demonstrated by the colored U^* contour lines in the entire compartment for any specified instant during impact. The calculated results are expected to improve the side impact crashworthiness to reduce the risk of injury to occupants.

As an example, to increase the load transfer of the cross-member under the front seat, we locate the stiffener member between the side sill and the tunnel structure. The designation of the stiffener location is pinpointed by the distribution of U^* . A crash simulation of a sample vehicle equipped with the stiffened cross-member reveals that the side sill intrusion deformation decreases by more than 30%. The value of the decrease rate itself is not a key point of the result. The point of importance is the effectiveness of the deduction process by U^* for the strict determination of structural improvement.

INTRODUCTION

Occurrence of traffic accidents is a social problem, and reduction of injuries to vehicle occupants is the inevitable research subject. Side impact accounts for a relatively large fraction of the total numbers of accidents

and fatal injuries.

In order to decrease injuries caused by side impacts, improvement of both the occupant protection system and the vehicle body structures is important. In the present study, we focus on the investigation of the vehicle body structure. Reduction of the intrusion velocity of the vehicle body-side structure into the compartment is the aim of the structural improvement ^{[1] [2]}. Understanding the load transfer from a moving deformable barrier (MDB) into the body structure is highly effective in increasing the stiffness of the compartment.

Load transfer in structures has been generally studied by examining the stress distribution ^[3]. However, observing the load transfer using stress distribution is rather difficult because of the effect of stress concentration around holes or notches. It is unreasonable to conclude that a hole or notch is effective for the load transfer. A novel index Ustar (U^*) previously developed by the authors has been used to express the load transfer and load paths, thereby overcoming the abovementioned problem of stress concentration ^[4].

The concept of U^* has been used in vehicle body structures ^{[5] [6]}. For the calculation of U^* under dynamic loading, a method has been proposed that includes the effect of inertial forces ^[7]. Previously, using this approach, we calculated the load transfer in a passenger car compartment during frontal collision ^[8].

Extending the study of frontal impact, in the present study, we introduce similar methods for side impact. We apply the index U^* to numerically depict the load transfer and load paths in a compartment structure during a side impact.

In the U^* calculation under side impact, the compartment structure except for the front-end structure of a finite element model is assumed to be elastic. As will be mentioned later, we also use the assumptions of a "dynamic-static method" and "equivalent inertial force method". Through application of these methods for the side impact of a sample passenger car, the obtained U^* distribution shows that the cross-member under the front seat should especially be stiffened. A dynamic crash simulation demonstrates the significant effectiveness of the newly stiffened cross-member.

METHODS

Index U^* and Load Transfer

The concept of the index Ustar (U^*) that was previously developed by the authors ^[4] is summarized as follows. Figure 1 shows a linear elastic body in which an external force p_A is applied at Point A. Point B is a support end, and Point C is an arbitrary point. The relationship between forces and displacements for these three points is

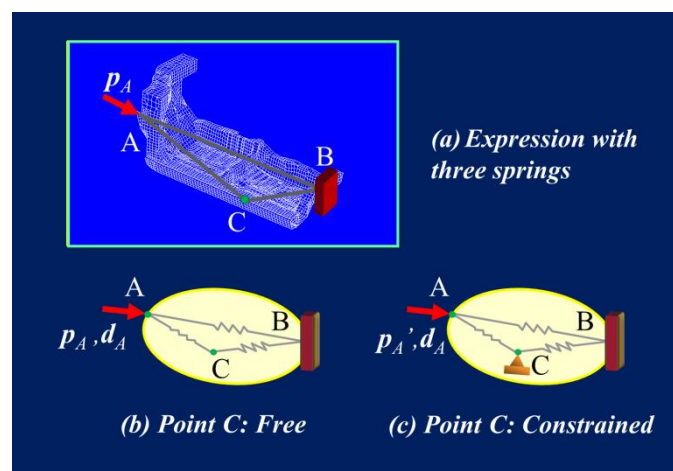


Figure1. Ustar calculation.

$$\begin{Bmatrix} \mathbf{p}_A \\ \mathbf{p}_B \\ \mathbf{p}_C \end{Bmatrix} = \begin{bmatrix} \mathbf{K}_{AA} & \mathbf{K}_{AB} & \mathbf{K}_{AC} \\ \mathbf{K}_{BA} & \mathbf{K}_{BB} & \mathbf{K}_{BC} \\ \mathbf{K}_{CA} & \mathbf{K}_{CB} & \mathbf{K}_{CC} \end{bmatrix} \begin{Bmatrix} \mathbf{d}_A \\ \mathbf{d}_B \\ \mathbf{d}_C \end{Bmatrix} \quad (1)$$

where \mathbf{K} , \mathbf{p} , and \mathbf{d} with suffixes are the internal stiffness tensor, force vector, and displacement vector, respectively. The expression of Eq. (1) is not the elementary formulation of the finite element method (FEM) but rather the representation of the overall behavior of an entire structure.

The work done by the force \mathbf{p}_A and the displacement \mathbf{d}_A at Point A in Fig. 1(b) is denoted as U . When Point C is constrained as shown in Fig. 1(c), the work done under the same displacement \mathbf{d}_A at Point A is denoted as U' . A non-dimensional value

$$U^* = 1 - \frac{U}{U'} \quad (2)$$

indicates the definition of the index U^* at an arbitrary point in the structure. The index U^* means the stiffness between the loading point A and an arbitrary point.

From Eqs. (1) and (2), we have

$$U^* = \left(1 - \frac{2U}{(\mathbf{K}_{AC} \mathbf{d}_C) \cdot \mathbf{d}_A} \right)^{-1} \quad (3)$$

where tensor and vector notations are employed instead of matrix notation for the products. The value of U^* is unity at the loading point A and zero at the support B. It can be seen that the index U^* is expressed by \mathbf{K}_{AC} which is a tensor value stiffness between the loading points and an arbitrary point. Although we can calculate Eq. (2) by FEM, the inspection load methods^[9] based on Eq. (3) can reduce the calculation time remarkably.

Load Path and Optimization

Figure 2(a) shows schematic U^* distributions and contour lines. The ridgeline of a three-dimensional curved surface is defined as the line that connects the highest points of stiffness in series from the loading point. We define this ridgeline as a load path because it can be regarded that the line that connects the highest stiffness points transfers the largest loading.

The actual U^* contour lines and the load paths are calculated for a simple plate model shown in Fig. 2(b). The stress concentration does not affect the load paths.

To confirm the concept of U^* being applicable to structures, an optimization process using a genetic algorithm (GA) for U^* was previously tested^[10]. In the optimization process, the objective function was determined based on the following three conditions for desirable structures.

- (a) Uniformity: Uniform decrease in U^* along a path (Fig. 3(a))
- (b) Continuity: Smoothness of the curvature of U^* along a path (Fig. 3(b))
- (c) Consistency: Coincidence between a path from Point A and a path from Point B (S_1 and S_2 in Fig. 3(c))

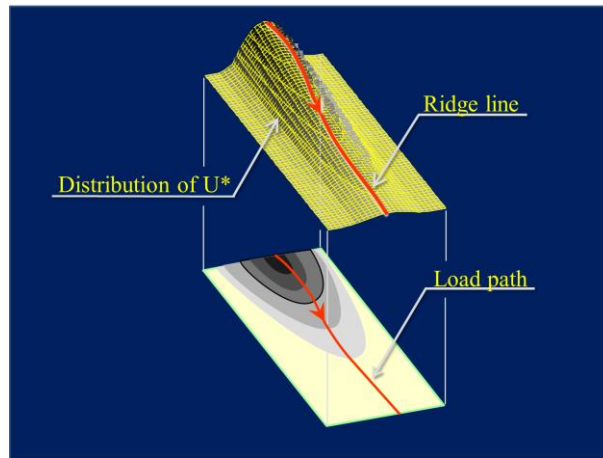
For the flat plate model shown in Fig. 4(a), the design parameter of optimization was the thickness of each element. The optimized structure obtained using U^* in the 50th generation of the GA is shown in Fig. 4(b). For comparison, the result of sensitivity analysis, which is one of the conventional optimization methods for strain energy density, is shown in Fig. 4(c). There is no significant difference in the thickness distribution, and this indicates the validity and effectiveness of the U^* theory.

During both the optimization processes, the thickness distribution developed once into the Michell truss pattern but then eventually attained a simple pattern using the operation of intensification.

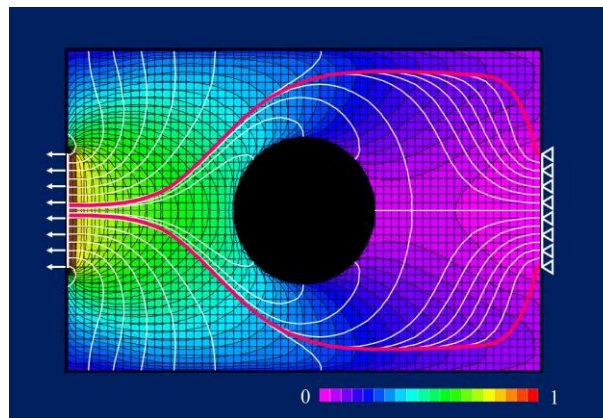
It is important to see that this objective function using U^* has no relationship to the concepts of stress. Generally, the concept of stress is suitable as the parameter of strength, and U^* is adequate for the index of load transfer.

Since the above reference is for the confirmation of the concept of U^* , hereafter we do not intend to

discuss the optimization in the present paper.



(a) Load path



(b) Distribution of U^*

Figure2. Definition of load path and distribution of U^* .

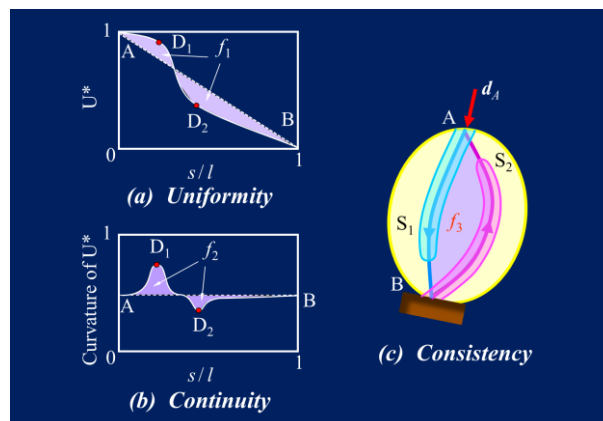


Figure3. Conditions of desirable structure.

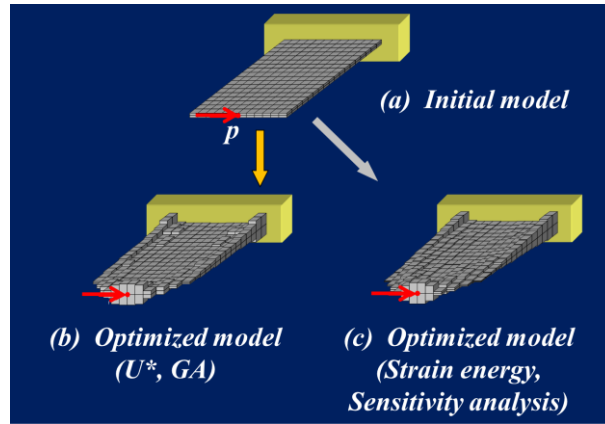


Figure4. Structural optimization.

Effect of Inertial Force

For the calculation of side impact, the definition of U^* under dynamic loading including the effect of inertial force is required. Since we already developed the calculation method of U^* under the effect of inertial force^[7], here, we present only the abbreviated summary.

Figure 1 shows the loading point A, support point B, and arbitrary point C. Here, for the inertial force, we introduce other points D_i ($i = 1, 2, 3, \dots, n$; n : number of nodes) shown in Fig. 5.

For simplicity, we consider the case of $n = 1$, which means that the inertial force is applied to only one node of a finite element. In Fig. 1, an elastic body with Points A, B, and C is expressed by three springs. Introducing the new Point D, we should use the six-spring model as shown in Fig. 6. For the new model, the definition of U^* is given as

$$U^* = \left\{ 1 - \frac{2U}{[(k_{AC} - k_{AD}k_{DD}^{-1}k_{DC})d_C] \cdot d_A} \right\}^{-1} \quad (4)$$

instead of Eq. (3), where k with suffixes expresses the internal stiffness tensor between two points. The suffixes represent the two related points. The stiffness in the six-spring model is different from the stiffness in the three-spring model: $k_{AC} \neq K_{AC}$.

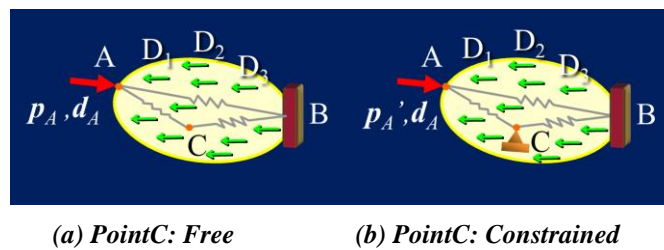


Figure5. Elastic structure with three springs.
(D_1, D_2, D_3, \dots : inertial forces)

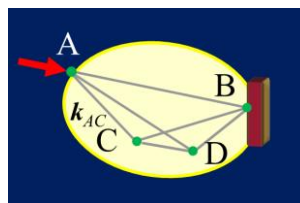


Figure6. Elastic structure with six springs.

For the case of zero inertial force, the U^* value of Eq. (3) should coincide with that of Eq. (4). Remembering that the displacement d_A or d_C can be given independently of the stiffness and that the stiffness is constant for a given structure, the following equation

$$K_{AC} = k_{AC} - k_{AD}k_{DD}^{-1}k_{DC} \quad (5)$$

is obtained. Equation (5) shows that it is unnecessary to calculate its right side; rather, it is sufficient to know the left side, which can be determined by the static U^* calculation using Eq. (4) with the inspection load method. However, in Eq. (4), we should adopt the value of d_C under dynamic loading.

FULL-WIDTH FRONTAL COLLISION ^[8]

Application of U^* to Frontal Collision

In our previous report ^[8], we applied the index U^* to the full-width frontal collision (56 km/h) for a sample vehicle structure. Since the index U^* is applied only for elastic structures, we used the following assumption of structural separation. Namely, we assumed the passenger compartment as an elastic body for the calculation of the load transfer by using U^* . The original material properties of the vehicle front-end crash region were not changed, and the rear end was assumed to be rigid (Fig. 7).

The dynamic crash behavior for the vehicle model was calculated by LS-DYNA. A deformed body at an arbitrary instant in the crash was extracted. The extracted compartment model was used for the static U^* calculation by MSC Nastran. The combined operation above using the dynamic simulation and static calculation is called the “dynamic-static method.”

The loading area for the static U^* calculation was located at the boundary between the front-end structure and the passenger compartment. The support area was located at the boundary between the compartment and the rear end (Fig. 8).

Equivalent Inertial Force

We used the abovementioned definition of U^* (Eq. (4)) under the dynamic condition. In this calculation, inertial

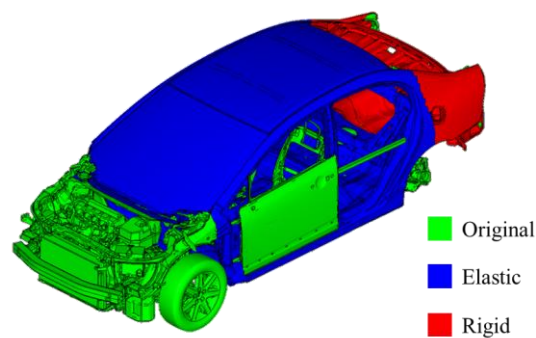


Figure7. Structure separation.

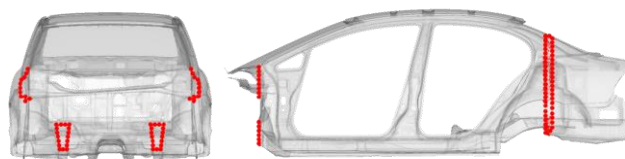


Figure8. Loading and support.

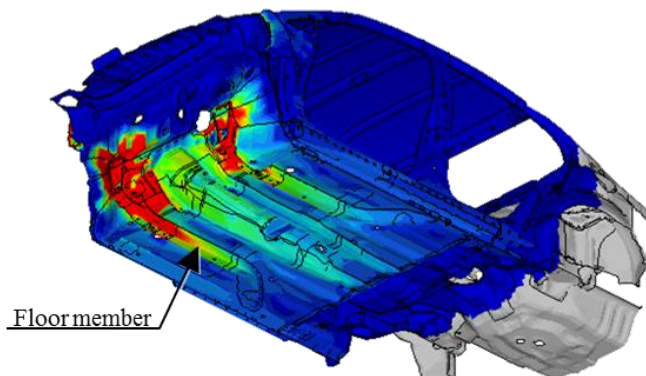
force should be applied to every FE node. Using the abovementioned dynamic-static method, we obtained displacement vectors of every node for the extracted compartment at any instant during collision. The necessary static force on each node for reproducing the obtained displacement was inversely calculated by NASTRAN. The necessary forces for such displacements from the initial configuration can be regarded as inertial forces. We call the present process the “equivalent inertial force method.”

Although the calculation of the above-described entire process requires complicated operation, automated software that had been developed beforehand was used.

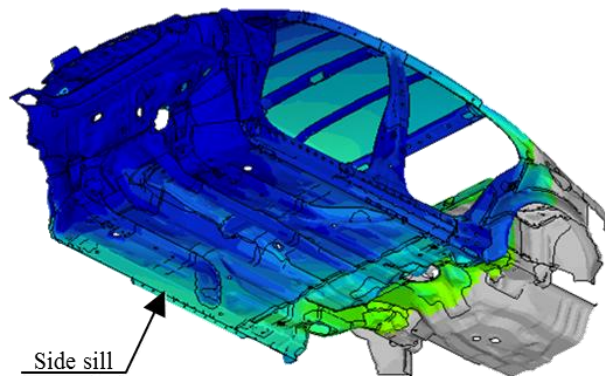
Load Transfer in Frontal Collision ^[8]

The load transfers from the front-end structure and the rear end are shown in Fig. 9 using U^* at 30 ms after frontal barrier collision. Although the maximum U^* value from the front-end structure is 1, we set the maximum value from the rear end to 0.034, which is decided by the ratio of the frontal force to the rear supporting force.

By inspecting the U^* value from the front-end structure shown in Fig. 9(a), we can see that the frontal loading is transferred mainly to the under-floor member. In contrast, as shown in Fig. 9(b), the supporting force from the rear end is transferred to the side sill. We call such a discrepancy the inconsistency of load paths (Fig. 3(c)). This discrepancy indicates that an increase in the stiffness of the connecting member between the under-floor member and the side sill is required.



(a) Distribution of U^* from loading area



(b) Distribution of U^* from support area



Figure9. Distribution of U^* (30ms).

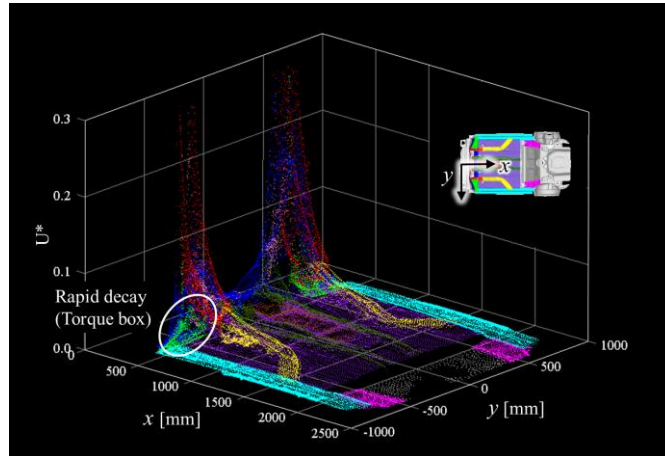


Figure10. Disutribution of U^* scatter diagrams (30ms).

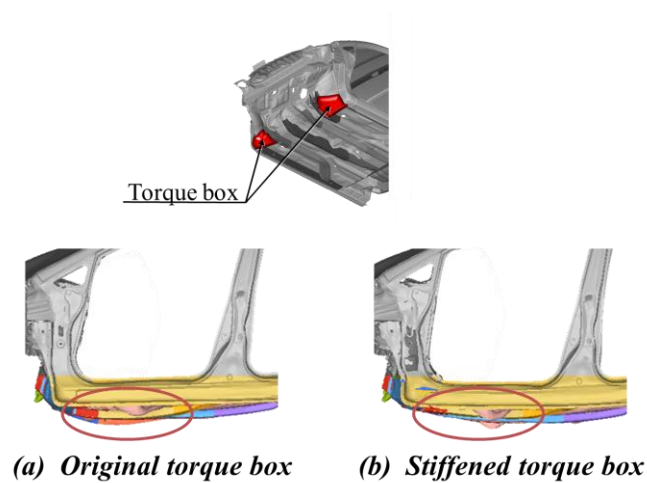


Figure11. Comparison of deformation ($\times 40$ deformation, 40ms).

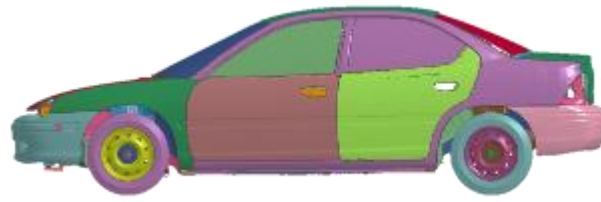
For a clearer observation, the scatter diagram of U^* is shown in Fig. 10, where the U^* value of each FE node is plotted on the x - y plane (x , y : longitudinal and lateral coordinates, respectively, of a compartment structure). The FE nodes of the connecting member (torque box) between the under-floor member and the side sill are indicated in the figure, which shows the rapid decrease in U^* along the connecting member.

Based on these results, the torque box was stiffened for a remodeled vehicle. The vehicle with such a stiffened body was calculated for the frontal impact by LS-DYNA. Comparison of deformation between the original body and the stiffened body is shown in Fig. 11. As expected, an undesirable large deformation of the under-floor member in the original body was improved by the use of the stiffened torque box.

SIDE IMPACT

Calculation Model

Application of the U^* calculation to side impact is the final goal of the present study. The FE model of a passenger car with 272,485 elements for side impact is shown in Fig. 12(a). The model type of the MDB is ECE-R95 (Fig. 12(b)). The impact speed is 55 km/h. For the dynamic and static calculations, LS-DYNA and MSC Nastran, respectively, are used. The loading area and the supporting area are shown in Fig. 13.



(a) Passenger car ^(#)



(b) Moving deformable barrier

^(#) National Crash Analysis Center, Dodge Neon, Detailed model,
Date posted: 2006 Jul. 3, available from
(<http://www.ncac.gwu.edu/vml/models.html>)

Figure12. Calculation model.

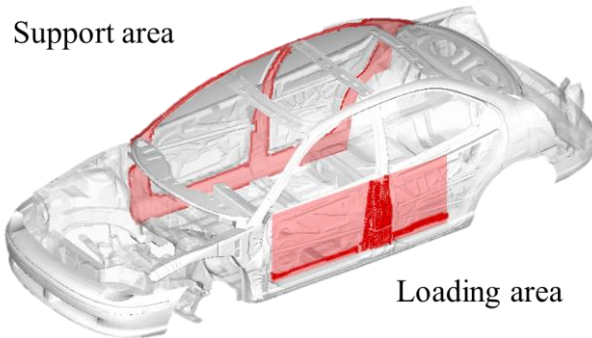


Figure13. Loading and support (Static U^* calculation).

Calculation Process

Since the U^* calculation is applied to only elastic bodies, as mentioned above, it is necessary to assume that the material property of the passenger compartment is elastic. However, based on the assumption of structural separation as shown in Fig. 14, the original material property is used for the outer panels of both the body sides of the compartment including doors as the crash area and the supporting area.

The dynamic vehicle behavior under side impact is calculated by LS-DYNA, and the deformation of the compartment structure at an arbitrary instant is extracted. In the same manner as described above for frontal collision, using the dynamic-static method, we statically calculate the extracted frozen compartment model to obtain the U^* distribution by MSC Nastran (Fig. 15).

For the definition of U^* under dynamic condition (Eq. (4)), the equivalent inertial force is applied to every FE node as the distributed external force in the static U^* calculation (Fig. 16). For retaining the deformation of the extracted compartment at any instant, the necessary static force on each node for reproducing the deformed shape of the body is conversely calculated by NASTRAN. The calculated forces can be regarded as the equivalent inertial forces.

Selection of U^* Theory

From the definition of U^* (U_{star}), the forced deformation at the loading points is constant during the calculation of load transfer. Namely, deformation is the parameter of the applied work. From the definition of

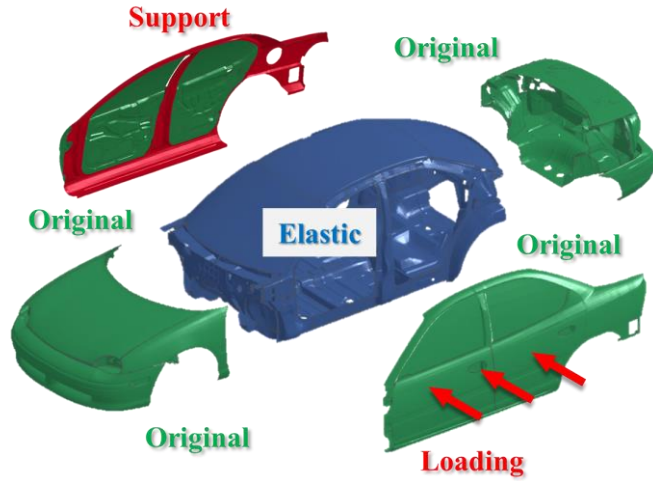


Figure14. Structure separation.

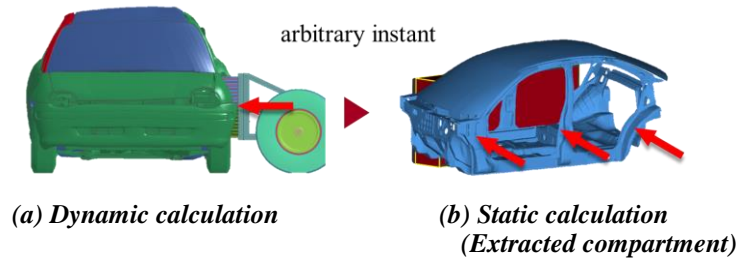


Figure15. Dynamic-static method.

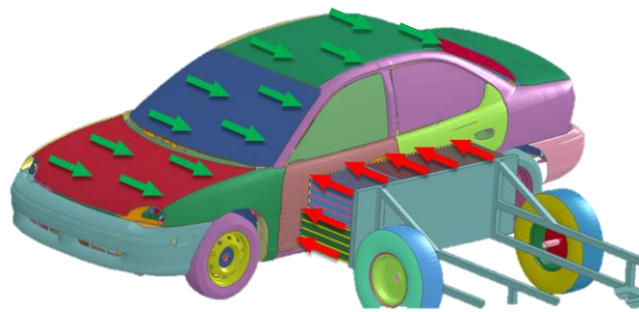


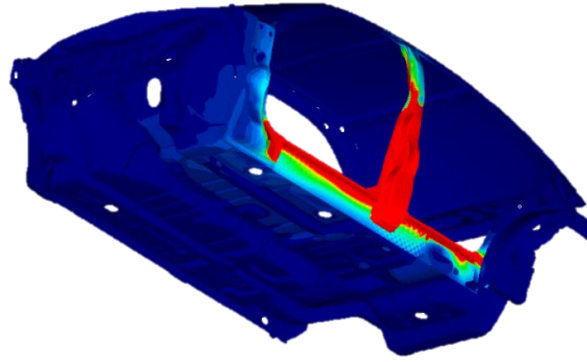
Figure16. Equivalent inertial force.

another index U^{**} (Ubistar), on the contrary, force at the loading points is constant during the calculation, wherein force is the parameter of applied complementary work ^[11].

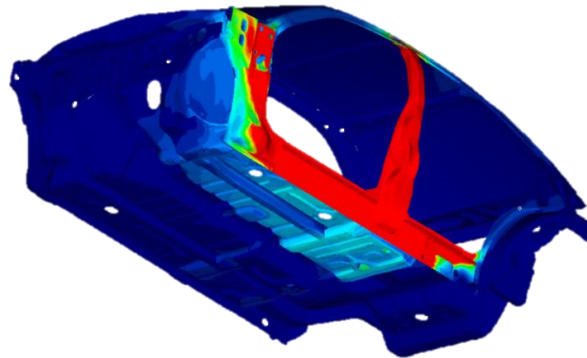
Since the MDB is equipped with an aluminum honeycomb, the applied force is almost constant during impact. Thus, for side impacts, application of U^{**} is more desirable than application of U^* . However, the MSC Nastran U^* Toolkit ^[12] saves calculation time, and FRONE U^* PRE ^[13] performs systematic dynamic calculation for U^* . For these reasons, here, we use the conventional U^* .

Load Transfer in Side Impact

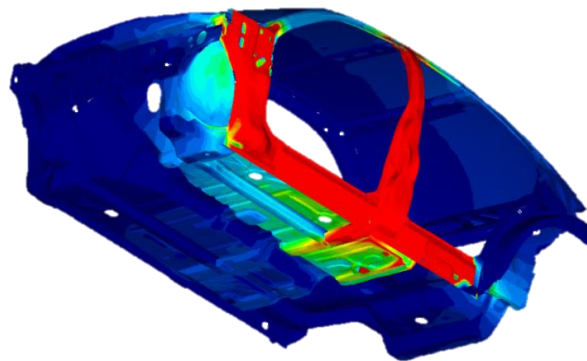
For the above passenger vehicle, U^* values from the loading area under side impact are shown in Fig. 17 for 10, 20, 30, and 40 ms after impact. From the definition of U^* , which is non-dimensionalized, the maximum value of U^* is 1 at any instant during a collision. However, to express the process during impact, the maximum



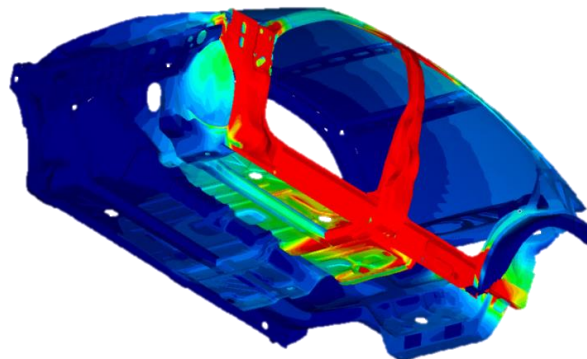
(a) 10ms (max: 1)



(b) 20ms (max: 17.4)



(c) 30ms (max: 87.1)



(d) 40ms (max: 121)

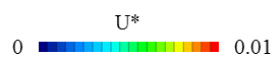


Figure17. Distribution of U^* from loading area during side impact.

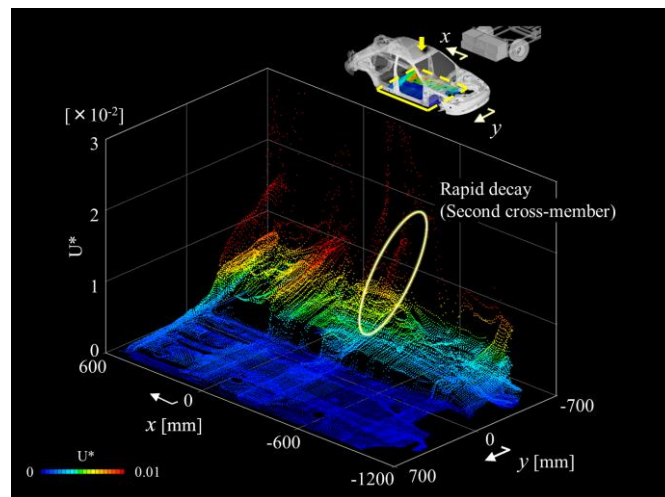
value of 1 is multiplied by the resultant crash force of each instant. The ratio of the resultant crash force is shown in the figure.

From Fig. 17, we can see that the input loading is transferred mainly to the lower structure. Despite the important role of the lower structure, the load transfer is interrupted by the tunnel structure. The floor structure is explicitly separated from the viewpoint of stiffness continuity, and the degree of separation is clearly represented by the U^* distribution.

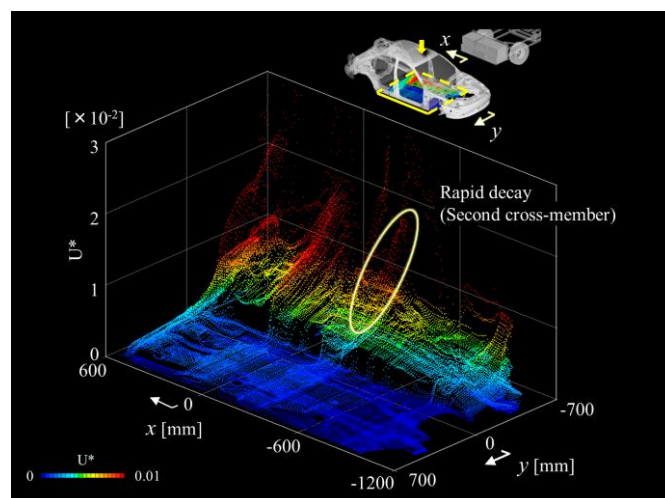
Figure 17 shows that among the several cross-members located across the floor panel, the cross-member located under the B-pillar is intensively effective. The impact force from the MDB presses the B-pillar strongly, and the force is transferred directly to the cross-member that is beneath the B-pillar.

On the other hand, the second cross-member that is located under the front seat has a small effect for the load transfer. Actually, by observing the scatter diagram in Fig. 18, which shows the U^* distribution of the lower structure, we can clearly see the rapid decay of U^* at the second cross-member.

The U^* distribution from the support end is shown in Fig. 19, which indicates the support capability of the opposite body side. Because of the existence of inertial force, the upper structure including the roof panel has relatively large U^* value. Figure 19 indicates that the upper structure has effective support capability, though the



(a) 30ms



(b) 40ms

Figure18. Disutribution of U^* scatter diagrams.

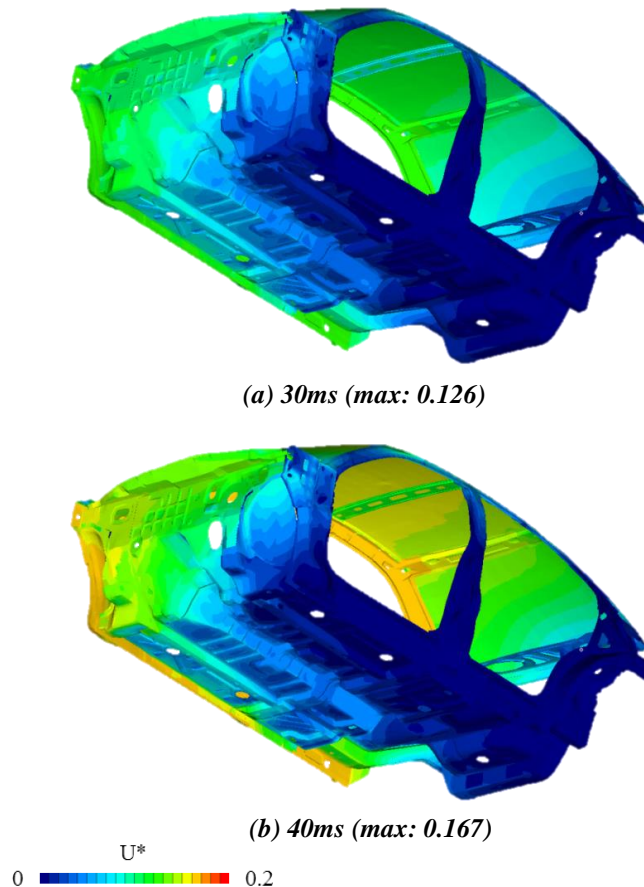


Figure19. Distribution of U^* from support area during side impact.

transferred impact force from the B-pillar to the roof panel is small.

STIFFENED CROSS-MEMBER

As shown above, the load transfer along the second cross-member located under the front seat is relatively small. To improve the stiffness of the second cross-member, we locate the stiffener member between the side sill and the tunnel structure. The beam model of a steel pipe (length: 606 mm, diameter: 48.6 mm, thickness: 3.2 mm) is used for the stiffener. The location of the pipe is shown in Fig. 20. The pipe end at the side sill is located at a point where the stiffness decreases rapidly.

The rapid decrease point of the stiffness is determined using U^* from the loading area (Fig. 20(a)). Another pipe end at the tunnel structure is decided by the rapid change point of U^* from the support (Fig. 20(b)).

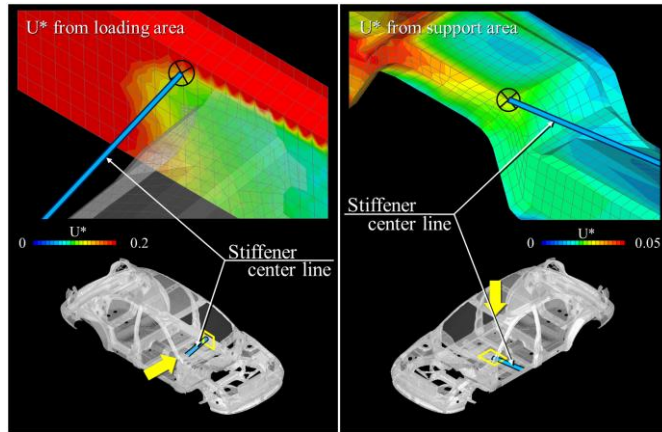
In general, for determining the location of a stiffener, it is necessary to connect the following two points:

- (1) the point with the maximum U^* from the loading area
- (2) the point with the maximum U^* from the support area

In the present study, we used the determination process of the stiffener location by inspecting the U^* distribution from both sides as a typical example of the above general application method of U^* .

Using the above stiffened body, we recalculated the side impact by LS-DYNA under the same crash condition as that for the original vehicle. The calculated result is shown in Fig. 21, where the side-sill intrusion deformation along the side sill upper edge at an instant 60 ms after the crash is plotted.

Although the maximum side sill intrusion deformation decreased by more than 30%, the value of the decrease rate itself is not a key point of the result. The point of importance is the effectiveness of the deduction



(a) Side sill

(b) Cross-member

Figure20. Stiffener location.

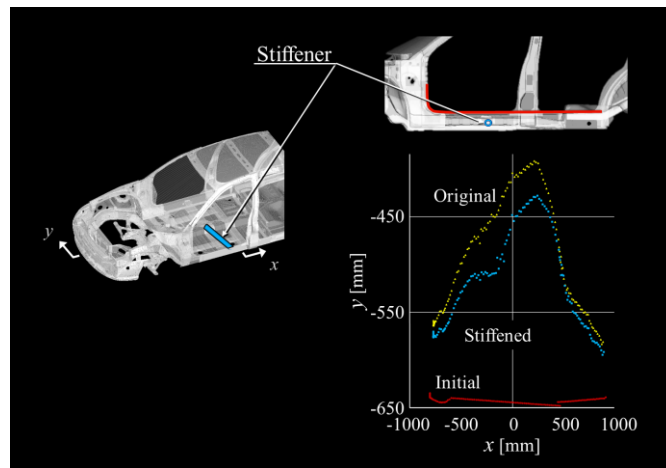


Figure21. Side sill intrusion (upper edge, 60ms).

process by using U^* for the strict determination of structural improvement.

CONCLUSIONS

With the aim of increasing the stiffness of a vehicle body structure in side impact, we investigated the load transfer and load paths into the passenger compartment from a moving deformable barrier (MDB) by using the new theory of Ustar (U^*).

- (1) The dynamic crash behavior for a sample vehicle model was calculated by a dynamic simulation. A deformed body at an arbitrary instant during the crash process was extracted, and the extracted compartment model was used for the U^* calculation by a static simulation.
- (2) The input loading to the sample vehicle structure is transferred mainly to the lower structure. Despite the important role of the lower structure, the load transfer is interrupted by the tunnel structure. The U^* distribution shows that in contrast to the effective cross-member located under the B-pillar, the cross-member under the front seat has only a small effect for the load transfer.
- (3) To improve the stiffness of the cross-member under the front seat, we located the stiffener member between the side sill and the tunnel structure. The designation of the stiffener location was pinpointed by inspecting the distribution of U^* . With the use of the stiffened body, the side sill intrusion

deformation improved by more than 30%.

ACKNOWLEDGEMENT

The authors would like to express their deepest gratitude to Prof. T. Maki, Prof. T. Sakurai, Mr. T. Iso, and Mr. Y. Zaiki for their helpful collaboration.

REFERENCES

- [1] Mangala, M. J., “2-Door Vehicle Body Local Force Evaluation with the IIHS, EuroNCAP and LINCAP Side Impact Barriers”, SAE Technical Papers, 2004-01-0333 (2004)
- [2] Abe, A., Sunakawa, T., Fujii, S., Fukushima, M. and Ogawa, S., “Aggressivity-Reducing Structure of Large Vehicle in Side Vehicle-to-Vehicle Crash”, SAE Technical Papers, 2005-01-1355 (2005)
- [3] Marhadi, K. and Venkataraman, S., “Comparison of Quantitative and Qualitative Information Provided by Different Structural Load Path Definitions”, *Int. J. Simul. Multidisci. Des. Optim.*, Vol.3, p.384-400 (2009)
- [4] Takahashi, K. and Sakurai, T., “Expression of Load Transfer Paths in Structures”, *Trans. JSME Ser. A*, Vol.71, No.708, p.1097-1102 (2005) (in Japanese)
- [5] Hoshino, H., Sakurai, T. and Takahashi, K., “Vibration reduction in the Cabins of Heavy-Duty Trucks Using the Theory of Load Transfer Paths”, *JSAE Review*, Vol.24, p.165-171 (2003)
- [6] Naito, T., Kobayashi, H., Urushiyama, Y. and Takahashi, K., “Introduction of New Concept of U*sum for Evaluation of Weight-Efficient Structure”, *SAE Int. J. Passeng. Cars – Electron. Electr. Syst.*, Vol.4, Issue 1 (2011)
- [7] Takahashi, K., Omiya, M., Iso, T., Zaiki, Y., Sakurai, T., Maki, T., Naito, T. and Urushiyama, Y., “Load Transfer Ustar (U*) Calculation in Structures under Dynamic Loading”, *Trans. JSME Ser. A*, Vol.79, No.807, p.1657-1668 (2013) (in Japanese)
- [8] Sakurai, T., Nonaka, D., Takahashi, K., Omiya, M., Naito, T., Urushiyama, Y. and Maki, T., “Application of Load Transfer Ustar Calculation to Cabin Structures under Frontal Collision”, *Proceedings of 2014 JSAE Annual Congress*, No.78-14, p.3-6 (2014) (in Japanese)
- [9] Sakurai, T., Takahashi, K., Kawakami, H. and Abe, M., “Reduction of Calculation Time for Load Path U* Analysis of Structures”, *Journal of Solid Mechanics and Materials Engineering*, Vol.1, No.11, p.1322-1330 (2007)
- [10] Kamimura, M., Hatta, Y., Ito, S., Koga, Y., Sakurai, T. and Takahashi, K., “Structural Optimization and Load Paths”, *Trans. JSME Ser. A*, Vol.74, No.737, p.6-12 (2008) (in Japanese)
- [11] Wang, E., Yoshikuni, Y., Guo, Q., Nohara, T., Ishii, H., Hoshino, H. and Takahashi, K., “Load Path U** Analysis of Truck Cab Structure under Frontal Collision”, *Proceedings of 2009 JSAE Annual Congress*, No.21-09, p.5-8 (2009)
- [12] MSC Nastran U*Toolkit, available from (<http://pages.mscsoftware.com/rs/mscsoftware/images/NastranUserMeeting-MSC-Ustar.pdf>), (accessed 2015-3-16)
- [13] FRONE U*PRE, available from (<https://drive.google.com/folderview?id=0B23OQ8Pgk40VX3hubUpJaXNFaTA&usp=sharing>), (accessed 2015-3-16)